Carbon nanocoils as catalysts support for methanol electrooxidation: A Differential Electrochemical Mass Spectrometry (DEMS) study

V. Celorrio [a,1], L. Calvillo [b], R. Moliner [a], E. Pastor [c], M.J. Lázaro [a,*]

[a] Instituto de Carboquímica (CSIC), Miguel Luesma Castán 4, 50018 Zaragoza, Spain
[b] School of Chemistry, University of Southampton, Highfield, Southampton SO17 1BJ, UK
[c] Universidad de La Laguna, Dpto. de Química-Física, Avda. Astrofísico Francisco Sánchez s/n, 38071 La Laguna (Tenerife), Spain

HIGHLIGHTS

- Carbon nanocoils (CNCs) were proposed as electrocatalysts support.
- Electrocatalyst' performance strongly depended on the synthesis method.
- CNCs-supported showed better electrochemical behaviour than E-TEK electrocatalysts.
- By using CNCs as support the reaction route of intermediates is favoured.
- Intermediates oxidation is facilitated by the use of CNCs as support.

ARTICLE INFO

ABSTRACT

Carbon nanocoils (CNCs) were used to prepare Pt and Pt–Ru catalysts by the sodium borohydride (BM), methanol (MM) and polyol (EGM) solution reduction methods. Their physicochemical properties were studied by means of energy dispersive X-ray analysis, X-ray diffraction and transmission electron microscopy, whereas the electrochemical activity towards carbon monoxide and methanol oxidations was studied using cyclic voltammetry and chronoamperometry. Furthermore, differential electrochemical mass spectrometry experiments were carried out to study the reaction mechanisms. Results were compared with those obtained for the commercial Pt/C and PtRu/C catalysts from E-TEK. It is shown that choosing an adequate synthesis procedure, better electrocatalytic behaviours towards CO and methanol oxidation can be obtained by using carbon nanocoils as support material.

1. Introduction

Direct methanol fuel cells (DMFCs) are promising power sources, especially for electric vehicles. Due to their low operating temperature (60–80 °C), vehicle emissions are significantly lower than those of conventional vehicles using internal combustion engines. However, its low activity compared with H_2/O_2 systems, currently being achieved with polymeric electrolyte membrane fuel cells (PEMFCs), is still an important drawback to be solved [1,2]. An important limitation of DMFCs is the low activity at the anode side; therefore, more efficient catalysts for the electrooxidation of methanol are urgently needed. The state of the art of electrocatalysts for methanol electrooxidation is centred on platinum-based nanoparticles supported on carbon black. Nowadays, only platinum-based catalysts reach the activity and stability required at the cathode and anode sides. So far, not noble metal-based catalysts have been found active enough for the oxidation of methanol. So, currently, the main objective is to reduce the amount of Pt maintaining or improving its catalytic activity [3–5].

During the methanol electrooxidation process, various reaction intermediates are formed, some of them CO-like species that act poisoning monometallic platinum electrodes at a concentration up to 10 ppm. For this reason, in the last few years, many efforts have been devoted to obtain more CO-tolerant electrocatalysts. It has been shown that the alloying of Ru, Sn or Mo with Pt provides more CO-tolerant anodes with better performance [6–8]. By using bimetallic alloys, CO tolerance has increased to values up to 100–200 ppm [9,10]. Among them, Pt–Ru alloys have shown to be the

* Corresponding author. Tel.: +34 976 733977; fax: +34 976 733318.
E-mail address: mlazaro@icb.csic.es (M.J. Lázaro).
[1] Present address: School of Chemistry, University of Bristol, Cantocks Close, Bristol BS8 1TS, UK.

most effective [11–17]. The presence of Ru facilitates the oxidation of CO species and, consequently, enhances the electrocatalytic activity for methanol oxidation. This effect is called bifunctional mechanism and/or "ligand effect" [4,17].

In Pt–Ru systems, some aspects such as the preparation procedure, the Pt:Ru atomic ratio and the metal-support interactions, have been found to strongly influence their performance for methanol oxidation. Antolini et al. [18] studied the effect of the catalyst composition in Pt–Ru alloyed catalysts supported on carbon. They concluded that catalysts with nominal Pt:Ru compositions in the range of 1:1–1:3 present the best performance in presence of CO, which is in good agreement with other authors like Takasu and Zhang [15,19]. The effects of the surface area of the carbon supports on the characteristics of Pt–Ru catalysts supported on different carbon blacks have been studied by Takasu et al. [19]. They showed that the extend of allowing, as well as the size of the $Pt_{50}Ru_{50}$ particles, decreased as the specific surface area of the carbon black increased, whereas the specific activity for methanol oxidation was enhanced. Therefore, the selection of a carbon support with suitable properties is very important to obtain an active electrocatalysts, since carbon materials have a strong influence on both the physicochemical and electrochemical properties of supported noble metal catalysts [20].

On the other hand, the catalyst synthesis method has also a strong influence on their activity, since the Pt:Ru atomic ratio, the particle size distribution and the metal dispersion can be controlled by changing the synthesis conditions. Therefore, different synthesis methods can result in catalysts with different characteristics [21,22]. There are three important methods to prepare carbon-supported Pt–Ru catalysts: impregnation-reduction, colloidal and microemulsion methods; although the colloidal method is the most extensively explored [11,23]. The high activity, the CO-tolerance reached and the possibility to control the particle size by using the colloidal method, make it an attractive alternative method to prepare electrocatalysts. However, it is still quite complicated and expensive compared to the impregnation-reduction one [14,24].

In this work we propose the use of carbon nanocoils as catalysts support for platinum and platinum-ruthenium electrocatalysts and the study of the effect that different reducing agents have on the catalyst properties. Pt and Pt–Ru electrocatalysts have been prepared by the solution-reduction method, using sodium borohydride, methanol or ethylene glycol. Their physicochemical properties have been studied by X-ray diffraction and transmission electron microscopy, whereas the electrochemical properties towards CO and methanol oxidation have been studied by cyclic voltammperometry and chronoamperometry. To complete the study, a comparison with commercial Pt/C and Pt–Ru/C catalysts from E-TEK is also reported. Furthermore, the electrocatalysts which presented the higher current densities were studied in a Differential Electrochemical Mass Spectrometer (DEMS) in order to understand their different electrochemical behaviours.

2. Experimental

2.1. Synthesis of carbon nanocoils (CNCs)

CNCs were synthesized by a low temperature procedure as described before [25]. Briefly, nickel (Panreac) and cobalt (Sigma–Aldrich) salts were added to an aqueous solution of formaldehyde (Sigma–Aldrich) and silica sol (Supelco) under stirring conditions. Then, resorcinol (Sigma–Aldrich) was added and the stirring was maintained for 30 min, being the molar ratios H_2O/Co salt/Ni salt/R/F/silica = 100:0.2:0.2:1:2:0.6. Afterwards, this mixture was subjected to a heat treatment at 85 °C during 3 h in a closed system, and then dried overnight at 108 °C. Finally, it was carbonized in

nitrogen atmosphere at 900 °C for 3 h. In order to remove the silica particles, the sample was treated with a 5 M NaOH (Panreac) solution and, subsequently, with concentrated HNO_3 (65%, Fluka) at room temperature during 2 h to remove the metal salts.

2.2. Preparation of the electrocatalysts

Pt and Pt–Ru supported electrocatalysts were prepared by the solution-reduction method, using different reducing agents, such as methanol (MM), sodium borohydride (BM) and ethylene glycol (EGM). These methods involve an impregnation step followed by a reduction step. In all cases, metal precursors (8 wt. % $H_2PtCl_6·6H_2O$ solution, Sigma–Aldrich, and 45–55% $RuCl_3$ Sigma–Aldrich) were dissolved and mixed with the carbon support and, subsequently, the metal precursors were reduced in situ.

In the case of the BM method, an aqueous solution of the metal precursors was prepared and mixed with the carbon support. Subsequently, sodium borohydride was slowly added to the solution at room temperature, in order to reduce the metal precursors [26].

In MM and EGM methods, precursors were dissolved in a 1:3 (v/v) methanol-water mixture and ethylene glycol, respectively. In these cases, methanol and ethylene glycol acted as both solvent and reducing agent. The syntheses were carried out at 90 and 195 °C for 2 h, respectively [21,27].

Appropriate concentrations of the precursors were used to obtain a theoretical metal loading of 20 wt.% and a Pt:Ru atomic ratio of 50:50.

2.3. Physicochemical characterization methods

The metal loading was determined by energy dispersive X-ray analyses (EDX) technique Röntec XFlash Si(Li), coupled to a scanning electron microscope Hitachi S-3400 N.

TEM studies were made using a JEOL-2000 FXII microscope, operated with an accelerating voltage of 200 kV.

X-ray diffraction (XRD) patterns were recorded using a Bruker AXS D8 Advance diffractometer with a $\theta–\theta$ configuration and using Cu Kα radiation (λ = 0.154 nm). Values of 2θ between 0° and 100° were recorded and Scherrer's equation was applied to the (220) peak of the Pt in order to estimate the crystallite sizes from the diffractograms [28].

2.4. Electrochemical studies

A two compartment electrochemical cell was used to carry out the electrochemical experiments using a MicroAutolab potentiostat. A large area pyrolitic graphite bar was used as counter electrode and a reversible hydrogen electrode (RHE) as reference. The reference and working electrodes were placed in different compartments connected by a Luggin capillary. All potentials in this paper are referred to the RHE reference electrode. A thin-layer of the electrocatalysts was deposited on a pyrolitic graphite disk (7 mm diameter, 1.54 cm^2 geometric area) to prepare the working electrodes. A mixture of 2 mg of the catalyst and 10 μl of Nafion dispersion (5 wt.%, Aldrich) in 500 μl of ultrapure water (Millipore Milli-Q system) was used to prepare the catalyst inks. A 40 μl aliqout of the suspension was deposited onto the graphite disk and dried in air. A 0.5 M H_2SO_4 (Merck) was used as electrolyte solution and was deaerated using nitrogen gas. All the electrochemical experiments presented in this work were carried out at room temperature.

Electrochemical active areas of the catalysts were determined by CO_{ads} stripping voltammetry using 20 mV s^{-1} scan rate, assuming the adsorption of a CO monolayer and a charge of

Table 1
Total metal content and Pt:Ru ratio obtained from EDX analysis.

Electrocatalyst	wt.% Total metal content	Pt:Ru
Pt/CNC-BM	20.0	−
PtRu/CNC-BM	17.3	66:34
Pt/CNC-EGM	16.2	−
PtRu/CNC-EGM	20.0	50:50
Pt/CNC-MM	20.1	−
PtRu/CNC-MM	20.0	74:26
Pt/C E-TEK	16.3	−
PtRu/C E-TEK	20.0	50:50

Table 2
Physical characteristics of the catalysts obtained from XRD analysis.

Electrocatalyst	(220) Diffraction peak position, 2θ (°)	Lattice parameter (Å)	d (nm)	Metal surface area (m^2 g^{-1})
Pt/CNC-BM	67.67	3.9198	4.7	60
PtRu/CNC-BM	67.94	3.9062	3.9	91
Pt/CNC-EGM	67.75	3.9158	5.6	50
PtRu/CNC-EGM	68.10	3.8981	3.8	94
Pt/CNC-MM	67.70	3.9184	4.8	58
PtRu/CNC-MM	68.40	3.8830	2.7	117
Pt/C E-TEK	67.53	3.9231	3.0	93
PtRu/C E-TEK	68.00	3.9031	3.4	82

420 μC cm^{-2} involved in the oxidation of CO$_{ads}$ [21,28]. These electroactive areas have been used to calculate the current densities given in the text.

Methanol oxidation was characterized by cyclic voltammetry using a scan rate of 20 mV s^{-1} and chronoamperometry in a 2 M CH$_3$OH + 0.5 M H$_2$SO$_4$ solution.

2.5. Differential electrochemical mass spectrometry (DEMS)

Working electrodes were prepared using gas diffusion electrodes (GDEs) of 7 mm diameter. First, a microporous layer of 0.8 mg cm^{-2} was prepared by mixing Vulcan XC-72R, ultrapure water (Millipore Milli-Q system), isopropanol (Merck, p.a.) and a PTFE dispersion (60 wt. %, Dyneon) and then deposited onto one side of a carbon cloth. Then, this carbon cloth was treated at 280 °C during 0.5 h and at 350 °C for 0.5 h.

Electrocatalyst inks were prepared by mixing the respective electrocatalysts with a Nafion dispersion (5 wt.%, Sigma−Aldrich) and ultrapure water (1:5:10 wt.) and deposited onto one side of the GDE. The final metal loading of the working electrodes was 0.7 mg metal cm^{-2}.

DEMS measurements were carried out in the experimental set-up described in Ref. [29]. Briefly, the working electrode is fixed between a PTFE membrane (Scimat) and a glassy carbon rod, which is connected to an Au wire to keep the electrical contact. Being the counter electrode a high surface area carbon rod and the reference electrode a reversible hydrogen electrode (RHE) placed inside a Luggin capillary. The potentiostat−galvanostat used was an Autolab PGSTAT302 (Ecochemie). The cell was directly attached to the vacuum chamber of the mass spectrometer (Balzers QMG112) with a Faraday cup detector. In this case, the scan rate used was 1 mV s^{-1} in order to avoid diffusional problems.

3. Results and discussion

### 3.1. Physicochemical characterization of the supports and electrocatalysts

The physicochemical characterization of the CNCs was stated in a previous work [25]. Carbon nanocoils presented a specific surface area of 124 m^2 g^{-1}, consisting on a long curved ribbon of carbon which exhibited well-aligned graphitic layers. On the other hand, commercial catalysts used for comparison are supported on Vulcan XC-72, which has a specific surface area around 250 m^2 g^{-1} and consists of an aggregation of 30−60 nm size-particles [30].

The metal content of the electrocatalysts was determined by EDX analysis. In all cases, the values obtained were closed to the nominal value of 20 wt.% (see Table 1). However, the Pt:Ru atomic
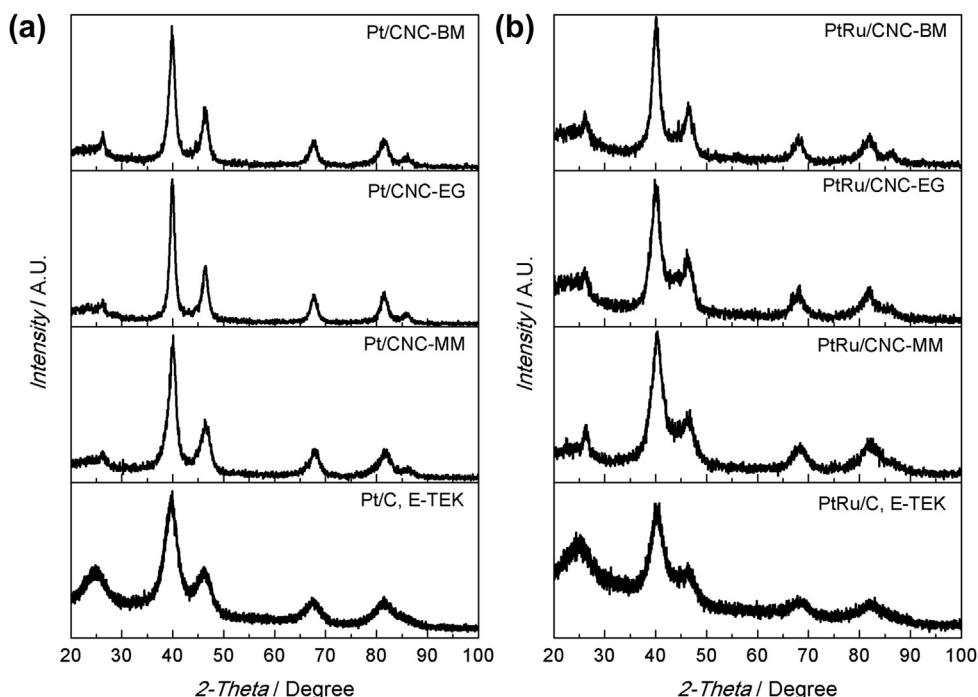
Fig. 1. XRD diffractograms for the Pt/CNC and PtRu/CNC catalysts synthesised by different methods and for the commercial Pt/C and PtRu/C catalysts from E-TEK.
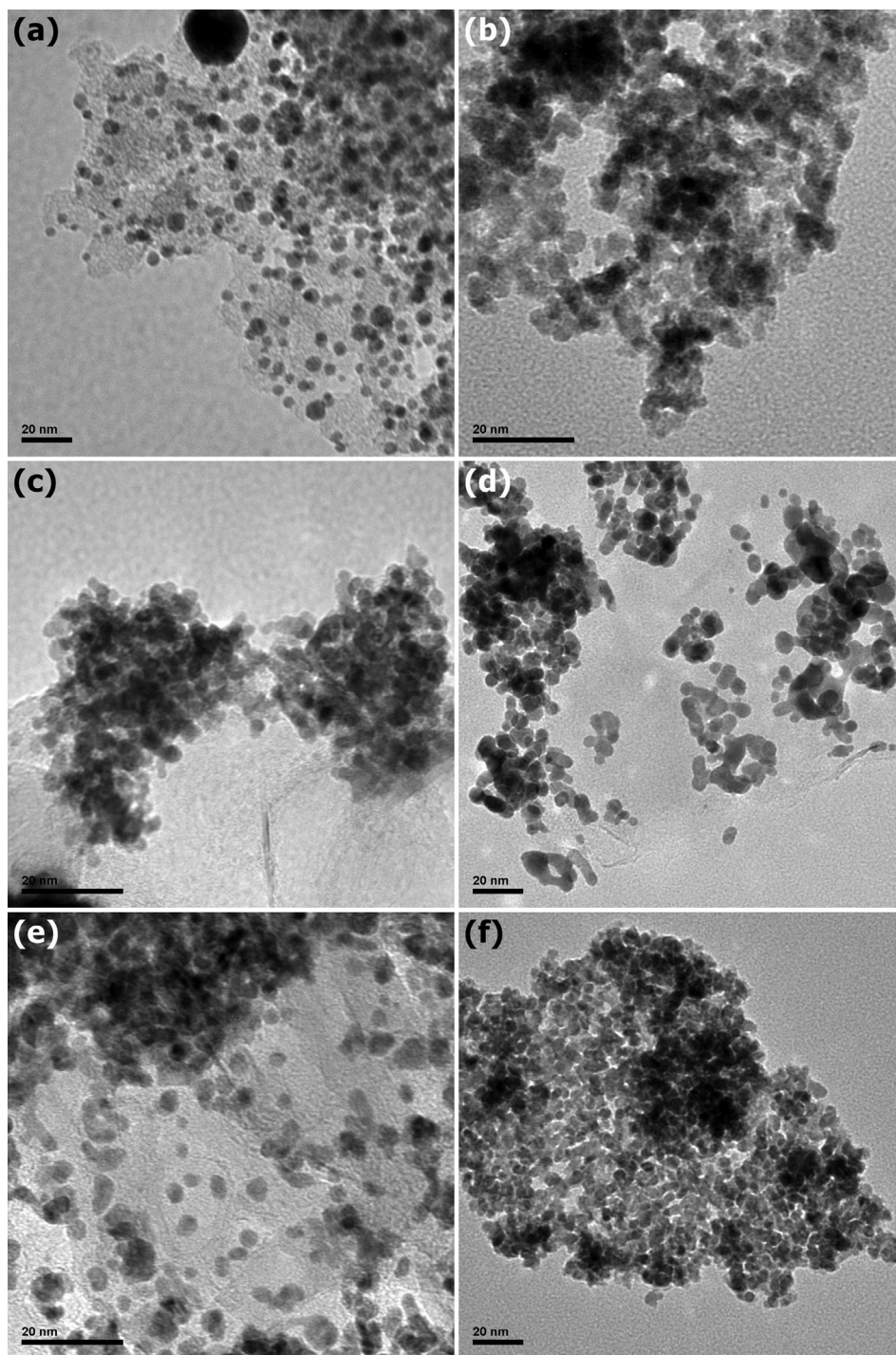
Fig. 2. TEM images of the Pt/CNC and PtRu/CNC catalysts synthesised by different methods: (a) Pt/CNC-BM; (b) PtRu/CNC-BM; (c) Pt/CNC-MM; (d) PtRu/CNC-MM; (e) Pt/CNC-EGM; and (f), PtRu/CNC-EGM.

ratio depended on the synthesis method. A good agreement between the theoretical and the experimental compositions was found with the EGM method. Nevertheless, for the BM and MM methods, the Pt:Ru ratios were 66:34 and 74:26, respectively, suggesting that the Ru precursor was not completely reduced under those synthesis conditions. It has already been demonstrated that many factors can affect the composition, morphology and dispersion of Pt–Ru/C catalysts when solution-reduction methods are used [17].

Fig. 1 shows the X-ray diffraction patterns for the Pt and Pt–Ru catalysts. The diffraction peak at $2\theta = 26°$ is attributed to the graphitic structure of the carbon materials used as support. In the case of Pt catalysts, the crystalline structure of the metal in the nanoparticles is evident and the XRD patterns clearly show the five characteristic peaks of the face-centred cubic (fcc) structure of Pt, namely (111), (200), (220), (311) and (222) planes. For the Pt–Ru catalysts, no peaks corresponding to metallic ruthenium with a hexagonal close packed (hcp) structure or ruthenium oxide phase
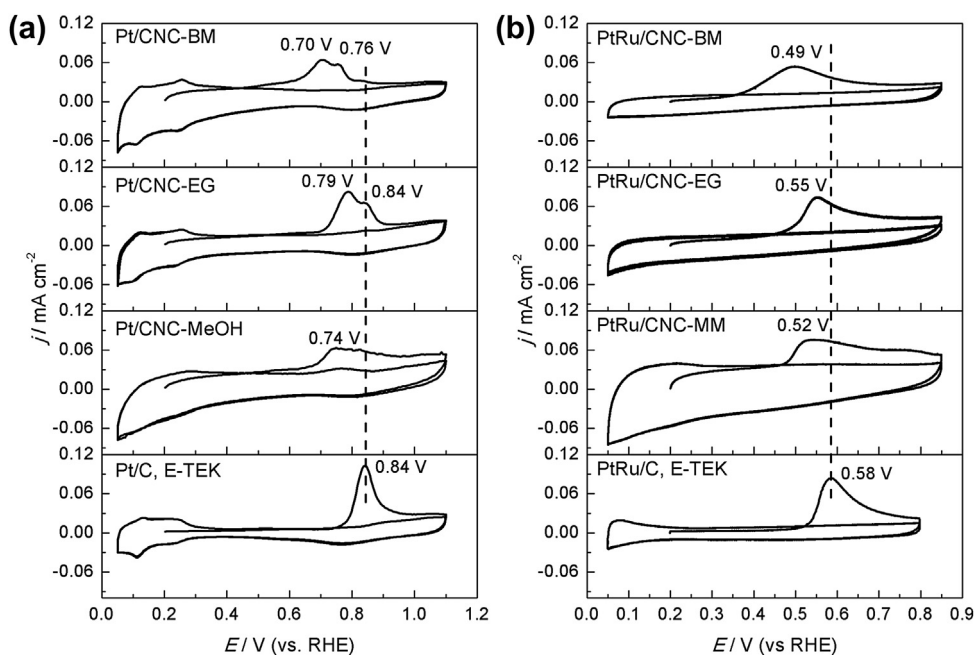
Fig. 3. CO$_{ads}$ stripping voltammograms for the platinum based (a) and platinum-ruthenium based (b) electrocatalysts. $E_{ad} = 0.20$ V; $v = 20$ mV s^{-1}; $T = 25$ °C.

were observed, indicating that Ru was incorporated in the Pt fcc structure.

Furthermore, it can be observed that the peaks for synthetized platinum catalysts were narrower than those for Pt–Ru catalysts, indicating larger metal particle sizes. This was confirmed by the calculation of the average metal crystallite sizes of the electrocatalysts using the Scherrer equation (Table 2). This result suggests that the addition of Ru species could inhibit the growth of Pt particles during the synthesis process [18]. In addition, the crystallite size depended on the synthetic route. The largest crystallite size was obtained by using the EGM, especially for Pt catalysts (5.6 nm for Pt/CNC).

It can be also observed that larger particles were obtained for catalysts supported on CNCs than for commercial ones (supported on Vulcan XC-72R). This could be attributed to the large number of nucleation sites that Vulcan XC-72R has, leading to the formation of smaller particles. In contrast, graphitized carbons, like CNCs, have a lower number of nucleation sites because only surface defects can act as nucleation sites, and thus larger metal particles would be obtained [21].

The lattice parameter was also calculated from the XRD patterns and the results are summarized in Table 2. The lattice parameters for PtRu/C catalysts were smaller than those for the corresponding Pt/C catalysts, indicating the introduction of Ru in the Pt fcc
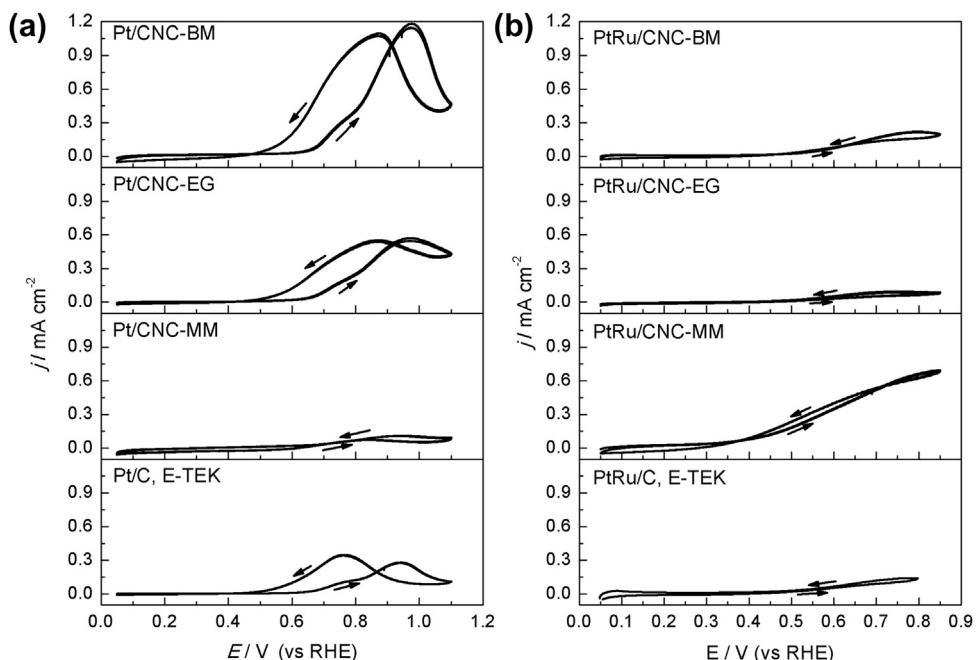

Fig. 4. CVs for platinum based (a) and platinum-ruthenium based (b) electrocatalysts in 2 M MeOH + 0.5 M H$_2$SO$_4$. $v = 20$ mV s^{-1}; $T = 25$ °C.

Table 3
Current densities obtained from cyclic voltammetry (CV) and chronoamperometric curves (CR) for Pt/C and PtRu/C catalysts in 2 M CH$_3$OH + 0.5 M H$_2$SO$_4$ solution at 0.60 V vs. RHE.

Electrocatalyst	CV$_{0.60}$ (μA cm^{-2})	CR$_{0.60}$ (μA cm^{-2})
Pt/CNC-BM	32	29
PtRu/CNC-BM	76	42
Pt/CNC-EGM	22	14
PtRu/CNC-EGM	54	8
Pt/CNC-MM	20	0.3
PtRu/CNC-MM	353	204
Pt/C E-TEK	10	14
PtRu/C E-TEK	66	74

structure producing an alloy. This result is in agreement with previous works and indicates the strong interaction between Pt and Ru forming an alloy [30].

TEM images of the Pt and PtRu catalysts supported on CNCs, synthesized by different methods, are given in Fig. 2. Metal particle sizes observed by TEM were in good agreement with those calculated from the XRD data. It can be observed that although a smaller particle sizes were obtained when Pt–Ru particles were prepared, samples seem more agglomerated. On the other hand, a good distribution of the metal particles on the support was obtained using the BM and EGM methods (Fig. 2a and e). However, the agglomeration of the metal particles was observed for Pt and PtRu catalysts prepared by the MM method (Fig. 2c and d).

3.2. Electrochemical studies

3.2.1. Carbon monoxide oxidation

In order to establish the CO tolerance of the catalysts, as well as the electroactive area, the adsorption and subsequent electrochemical oxidation on the catalysts of a CO monolayer has been carried out. CO stripping voltammograms were obtained after bubbling CO through the electrolyte solution for 10 min applying a potential of 0.2 V (vs. RHE), followed by nitrogen purging for removing the CO from the solution. Fig. 3 shows the CO-stripping voltammograms obtained at room temperature for Pt and Pt–Ru catalysts.

CO$_{ads}$ stripping peak for the commercial Pt catalyst from E-TEK occurred at around 0.84 V, whereas no CO oxidation peak was monitored in the second scan confirming the complete removal of the CO$_{ads}$ species. A shift to more negative potentials was observed when carbon nanocoils were used as support material. As a first approximation, this effect can be ascribed to the increase in Pt particle size. Smaller particle sizes have been ascribed to more

positive potentials of the CO stripping peak [31–34], due to the difficulty to form oxidized Pt sites with decreasing particle size.

On the other hand, Pt/CNC-BM and Pt/CNC-EGM samples presented two peaks. The more positive one, equivalent to that observed for the commercial catalyst, is observed at 0.73 V, whereas the peak at more negative potential was previously ascribed to particle agglomeration [32,33,35] as seen in Fig. 2. Enhanced catalytic activity of Pt agglomerates has been associated to grain boundaries, which interconnect nanoparticles into complex extended structures and are considered to contain active sites for fuel cell reactions. Pt/CNC-MM only presented one CO oxidation peak around 0.74 V, however, it can be observed that a great part of the CO$_{ads}$ is oxidized at higher potentials ($E > 0.86$ V) due to the worst particle dispersion observed for this sample in the TEM analysis. It can be then affirm that metal dispersion plays also a key role.

With the addition of Ru, the hydrogen adsorption/desorption region area of the voltammogram decreased and a shift of the oxide stripping peak to more negative potentials was produced. The CO$_{ads}$ oxidation peak for Ru-containing catalysts appeared at approximately 0.50 V, about 0.20 V more negative compared with Pt. The oxidation of CO on the commercial PtRu/C catalyst from E-TEK was found to begin at 0.52 V and attained a peak at 0.58 V. For catalysts supported on carbon nanocoils, both the onset and the peak potentials were shifted towards more negative potentials, respect to the commercial catalyst. The comparison between the different PtRu catalysts is rather difficult, since different Pt:Ru ratios were obtained. In the literature, the shift of the oxidation peak potential to more negative potentials as the Ru content increases has been reported [9]. For the catalysts studied in this work, it was observed that CO$_{ads}$ was more easily oxidized on the catalyst synthesised by the BM method (PtRu/CNC-BM), as happened for Pt catalysts, although it had a lower Ru content than expected (Pt:Ru ratio = 66:34). In this case, the onset potential occurred at 0.35 V and the CO oxidation peak was attained at 0.49 V.

Therefore, either for Pt or Pt–Ru catalysts, it was found that CO was more easily oxidized on catalysts prepared by the sodium borohydride method. This behaviour could be attributed to a slightly hydrogenation of the CNC surface during the reduction of the metal precursors, that could act promoting the oxidation of CO [36]. These results confirm the influence of the catalyst synthesis method and the use of carbon nanocoils as support on the CO oxidation reaction.
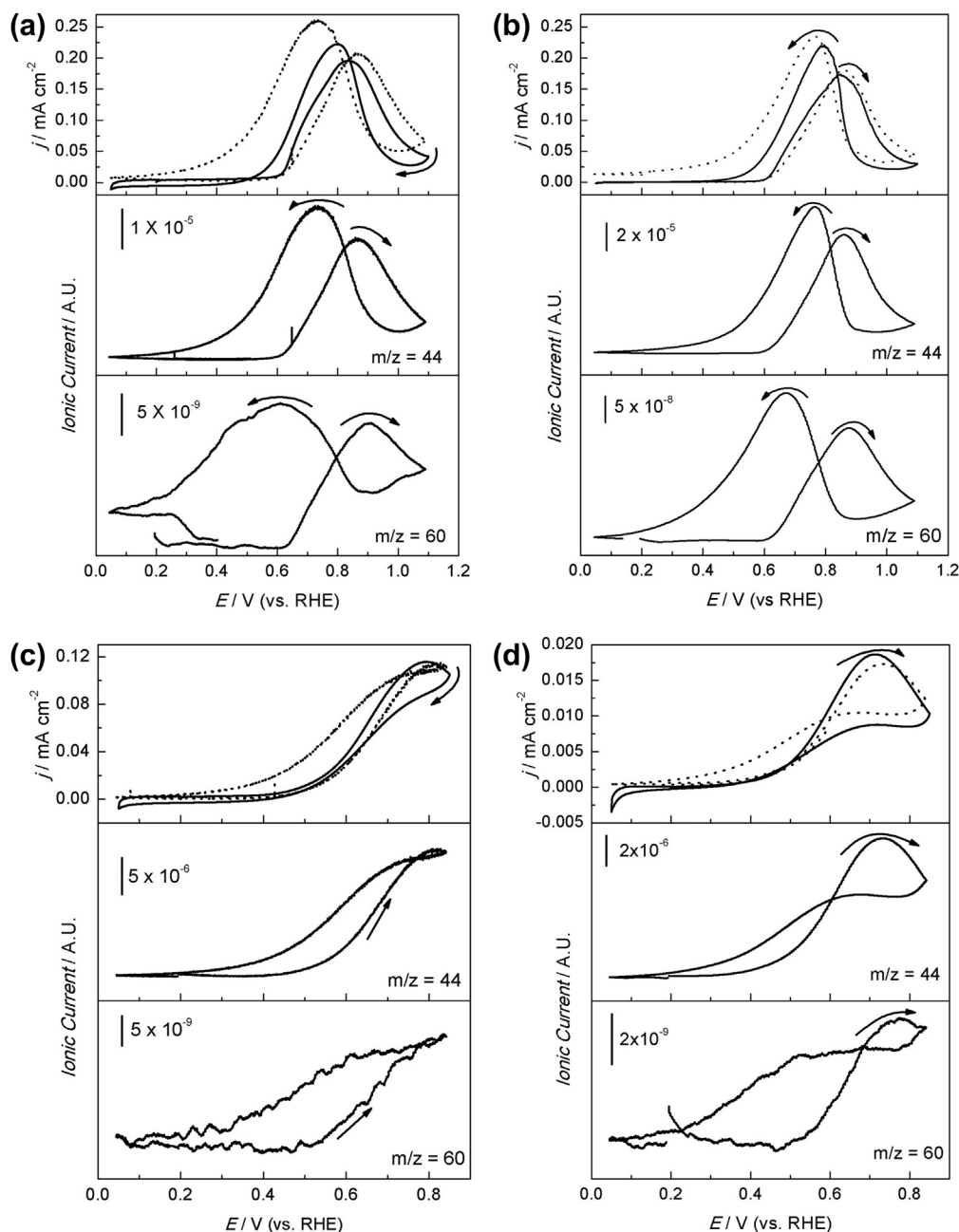
3.2.2. Methanol oxidation

Fig. 4 illustrates cyclic voltammograms recorded at room temperature for the catalysts studied in this work in a 2 M CH$_3$OH + 0.5 M H$_2$SO$_4$ solution.
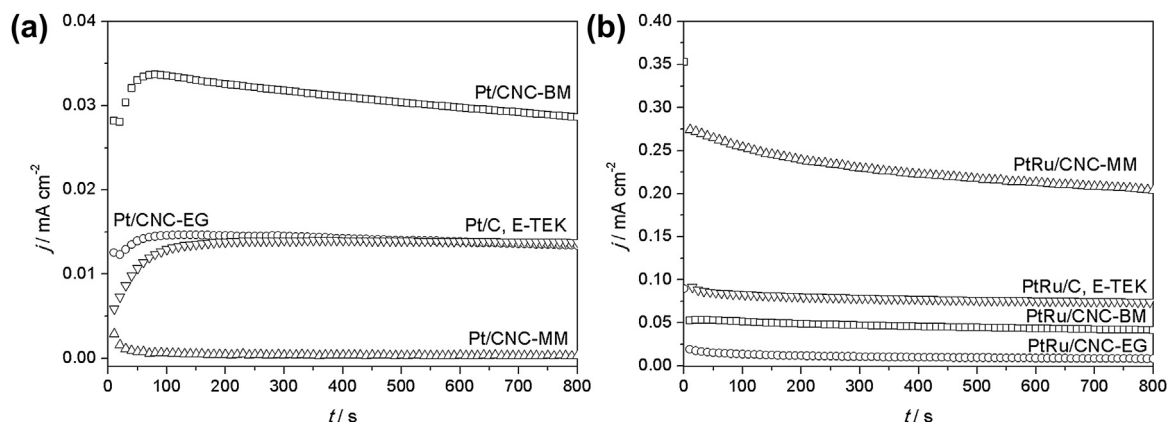
Fig. 5. *j/t* response recorded at 0.60 V vs. RHE in 2 M MeOH + 0.5 M H$_2$SO$_4$ for platinum based (a) and platinum-ruthenium based (b) electrocatalysts. *T* = 25 °C.

Fig. 6. CVs and MSCVs for 0.5 M CH$_3$OH oxidation in 0.5 M H$_2$SO$_4$ at Pt/CNC-BM (a), PtRu/CNC-MM (b), Pt/C E-TEK (c) and PtRu/C E-TEK (d) electrocatalysts. $v = 1$ mV s^{-1}; $T = 25$ °C.

Pt based catalysts (Fig. 4a) presented the irreversible behaviour for the methanol electrooxidation, the onset potential occurred at around 0.60 V vs. RHE for all them. Watanabe et al. [35] examined the influence of platinum crystallite dispersion on the electrocatalytic oxidation of methanol, affirming no crystallite size effects (even for crystallites as small as 1.4 nm diameter). For this reason, our results are entirely comparable. The highest current density was achieved by the Pt/CNC-BM catalyst during the positive scan at potentials around 0.98 V, corresponding to the methanol oxidation. This result could be associated to the higher CO tolerance of this catalyst, as shown above. Another peak at around 0.85 V was observed during the backward scan, which is attributed to the reactivation of the surface after Pt oxide reduction. Pt/CNC-BM also exhibited the highest current density at 0.60 V vs. RHE (potential near to the working potential in a DMFC). These specific activities

from CVs are summarized in Table 3. The current density for the methanol oxidation on the Pt/C E-TEK reached a value of 10 μA cm^{-2}, whereas the Pt catalysts supported on carbon nanocoils presented current densities two (Pt/CNC-EGM and Pt/CNC-MM) or three (Pt/CNC-BM) times higher. Pt/CNC catalysts showed higher activity towards methanol electrooxidation than the commercial Pt/C catalyst. This behaviour could be attributed to the carbon−platinum interaction, which could also be favoured by the presence of more oxygen groups on the surface of carbon nanocoils than on Vulcan (see reference [25]). These oxygen groups could help to oxidize the CO adsorbed on the Pt particles, thus increasing the efficiency of the catalysts in the methanol oxidation. From these result, it could be stated that the CO oxidation would be the limiting step, since the improvement of this path results in an improvement of the global process.

Methanol electrooxidation was also evaluated by chronoamperometry. Fig. 5 shows the potentiostatic current densities, normalized by the electroactive surface area, as a function of time at 0.60 V vs. RHE. The response increases in the order: Pt/CNC-MM < Pt/C E-TEK ~ Pt/CNC-EGM < Pt/CNC-BM (Table 3). These values follow the same trend than that observed before by cyclic voltammetry.

For Pt–Ru catalysts the onset potential, potential where the faradaic current starts rising, varied between 0.3 and 0.5 V (Fig. 4b), taking place a shift to more negative potentials respect to the corresponding Pt catalysts. In this case, the PtRu/CNC-MM catalyst showed the highest activity towards the methanol oxidation. For this catalyst, the current density grew faster than for the commercial PtRu/C from E-TEK. It was found that PtRu/CNC-MM catalyst displayed about 5-fold higher current density than the commercial PtRu/C catalyst at 0.60 V from the CVs (see Table 3). This result is in agreement with that published by Jusys et al. [37] confirming that at positive potentials (0.6–0.65 V) the Pt-rich catalysts are more active in the MOR. The chronoamperometric current density values increased in the following order: PtRu/CNC-EGM < PtRu/CNC-BM < PtRu/C E-TEK < PtRu/CNC-MM. For all of them, the values reached were higher than those for the corresponding Pt catalysts.

3.3. DEMS measurements

According to the electrochemical results previously described, DEMS experiments were performed in order to clarify the different behaviours observed with the supported Pt and PtRu catalysts. Pt/CNC-BM and PtRu/CNC-MM samples were chosen to be analysed by DEMS in order to explain their better behaviour compared with the commercial catalysts.

Fig. 6 shows the CVs (solid line) for the Pt/CNC-BM (a), Pt/C E-TEK (b), PtRu/CNC-MM (c) and PtRu/C E-TEK (d) and the corresponding mass signals for CO_2 ($m/z = 44$) and formic acid (followed through methylformate formation, $m/z = 60$) during methanol electrooxidation. In the upper panel, the faradic current expected for a 100% efficient conversion of methanol to CO_2, calculated from the $m/z = 44$ signal after calibration, was also included (dashed line). The difference in area between experimental (solid curve) and theoretical (dashed curve) currents is the extra charge associated with the formation of products different from CO_2 (formic acid can be indirectly detected by DEMS, but not formaldehyde).

In the case of the platinum-supported electrocatalysts, the $m/z = 44$ ion current (middle panels) generally traces the faradaic methanol oxidation reaction (MOR) current, taking into account the time constant of the DEMS cell. A closer comparison of Faradaic (black line, upper panels) and $m/z = 44$ ion currents reveals, that the ratio in MOR current depends on the potential scan direction, with relatively higher mass spectrometric currents in the negative-going scan. Also the MSCVs for methylformate formation ($m/z = 60$) largely follows the Faradaic current for MOR. However, the separation between the positive- and negative-going potential scans is larger compared with the $m/z = 44$ mass signal, although the time constant should be essentially the same. This deviation could be explained by the relative slow ester formation reaction between

formic acid and methanol compared to the instantaneous CO_2 formation [37].

Regarding to the PtRu-supported electrocatalysts, the formation of CO_2 starts at 0.4 V, i.e. about 200 mV more negative than that of Pt, whereas the formation of methylformate starts at 0.5 V, which is the same as in the case of Pt.

A more accurate comparison between the electrodes is possible from the faradic and ion-charge integrations during the forward scans of the CV and MSCV for CO_2. The average efficiency for each catalyst can be calculated on the bases of these integrated values and is present in Table 4. As can be seen, CO_2 efficiencies for the electrocatalysts supported on carbon nanocoils are lower than that for the commercial catalysts. However, the current densities achieved after 800 s in the oxidation of 2 M CH_3OH + 0.5 M H_2SO_4 (see Table 3) were higher. Therefore, it can be suggested that the use of CNC as electrocatalyst support facilitates the oxidation of methanol, indicating that the oxidation of methanol on the Pt/CNC-BM catalyst occurs through the reaction route of intermediates. Pt-CNC interactions promote the oxidation of CO_{ads}, whereas they do not help to oxidize the intermediaries, therefore the current densities obtained are lower. For the PtRu/CNC-MM catalyst, however, the current density reached after 800 s in the potentiostatic experiments was higher. Thus, it can be deduced that the use of CNC as support of Pt–Ru nanoparticles facilitates the oxidation of reaction intermediates. An increase in activity of Pt–Ru particles by being supported in carbon materials was already reported [28].

4. Conclusions

Carbon nanocoils have been proposed as alternative material that could replace carbon blacks as electrocatalyst's support for low temperature fuel cells. Pt and PtRu catalysts were supported on this carbon material by the solution-reduction method using different reducing agents, and their behaviour was compared with that of commercial Pt/C and PtRu/C catalysts from E-TEK. The results showed that an increase of the electrocatalytic activity can be obtained by using carbon nanocoils as electrocatalyst support and that the use of different synthesis conditions can affect the physicochemical and electrochemical properties of the catalysts.

For Pt catalysts, larger particle sizes were obtained using CNCs as support, compared with the commercial catalyst, getting the biggest particle size by the EGM method. On the contrary, for PtRu catalysts, similar particle sizes were obtained using CNCs as support, compared with the commercial catalyst from E-TEK. In this case, the smallest particle size was obtained by the MM method. Therefore, it can not be conclude that one method is better than the other ones, since the effect of the synthesis method depends also on the metals deposited.

The electrocatalysts performance also depended on the synthesis method. The catalysts synthesised by the BM method (Pt/CNC-BM and PtRu/CNC-BM) oxidized the CO_{ads} at more negative potentials than the rest of catalysts. This could be attributed to the slight hydrogenation of the carbon surface during the metal reduction step with sodium borohydride which promote the oxidation of carbon monoxide.

For the methanol oxidation, higher current densities were obtained on Pt/CNC electrocatalysts than on Pt/C from E-TEK. Taking into account that the commercial catalysts had smaller metal particle size, this result is attributed to the surface oxygen groups of carbon nanocoils, created during the HNO_3 treatment, which help to oxidize the CO adsorbed on Pt particles. The addition of Ru to Pt markedly increased the electrocatalytic activity towards methanol oxidation through the adsorption of oxygenated species on Ru-sites. The highest current densities were recorded for the PtRu/CNC-MM catalyst. However, a proper comparison between all

Table 4
Calculated average efficiency to CO_2.

Electrocatalyst	CO_2 conversion efficiency (%)
Pt/CNC-BM	97
PtRu/CNC-MM	85
Pt/C E-TEK	100
PtRu/C E-TEK	94

PtRu catalysts could not be carried out due to their different Pt:Ru atomic ratio.

Although lower CO_2 efficiencies were obtain for the electrocatalysts supported on carbon nanocoils by the DEMS measurements, better behaviour in the methanol oxidation reaction was observed for them. This fact suggest that although methanol oxidation is taking place through the intermediate pathway, the metal-CNC interaction facilitates the oxidation of methanol compared with the commercial catalysts.

Acknowledgements

References

[1] J.M. Andújar, F. Segura, Renewable and Sustainable Energy Reviews 13 (2009) 2309−2322.
[2] S.K. Kamarudin, F. Achmad, W.R.W. Daud, International Journal of Hydrogen Energy 34 (2009) 6902−6916.
[3] A.M. Zainoodin, S.K. Kamarudin, W.R.W. Daud, International Journal of Hydrogen Energy 35 (2010) 4606−4621.
[4] A.S. Aricò, S. Srinivasan, V. Antonucci, Fuel Cells 1 (2001) 133−161.
[5] T. Iwasita, Electrochimica Acta 47 (2002) 3663−3674.
[6] N. Tsiouvaras, M.V. Martínez-Huerta, O. Paschos, U. Stimming, J.L.G. Fierro, M.A. Peña, International Journal of Hydrogen Energy 35 (2010) 11478−11488.
[7] J.H. Kim, S.M. Choi, S.H. Nam, M.H. Seo, S.H. Choi, W.B. Kim, Applied Catalysis B: Environmental 82 (2008) 89−102.
[8] L.C. Ordóñez, P. Roquero, P.J. Sebastian, J. Ramírez, International Journal of Hydrogen Energy 32 (2007) 3147−3153.
[9] E.M. Crabb, M.K. Ravikumar, D. Thompsett, M. Hurford, A. Rose, A.E. Russell, Physical Chemistry Chemical Physics 6 (2004) 1792−1798.
[10] S.J. Lee, S. Mukerjee, E.A. Ticianelli, J. McBreen, Electrochimica Acta 44 (1999) 3283−3293.
[11] U.A. Paulus, U. Endruschat, G.J. Feldmeyer, T.J. Schmidt, H. Bönnemann, R.J. Behm, Journal of Catalysis 195 (2000) 383−393.
[12] J. Solla-Gullón, F.J. Vidal-Iglesias, V. Montiel, A. Aldaz, Electrochimica Acta 49 (2004) 5079−5088.
[13] W.-X. Chen, J.Y. Lee, Z. Liu, Materials Letters 58 (2004) 3166−3169.
[14] A.J. Dickinson, L.P.L. Carrette, J.A. Collins, K.A. Friedrich, U. Stimming, Electrochimica Acta 47 (2002) 3733−3739.
[15] Y.J. Zhang, A. Maroto-Valiente, I. Rodriguez-Ramos, Q. Xin, A. Guerrero-Ruiz, Catalysis Today 93−95 (2004) 619−626.
[16] Z. Qi, A. Kaufman, Journal of Power Sources 113 (2003) 115−123.
[17] H. Liu, C. Song, L. Zhang, J. Zhang, H. Wang, D.P. Wilkinson, Journal of Power Sources 155 (2006) 95−110.
[18] E. Antolini, L. Giorgi, F. Cardellini, E. Passalacqua, Journal of Solid State Electrochemistry 5 (2001) 131−140.
[19] Y. Takasu, T. Kawaguchi, W. Sugimoto, Y. Murakami, Electrochimica Acta 48 (2003) 3861−3868.
[20] L. Calvillo, V. Celorrio, R. Moliner, M.J. Lázaro, Materials Chemistry and Physics 127 (2011) 335−341.
[21] M.J. Lázaro, V. Celorrio, L. Calvillo, E. Pastor, R. Moliner, Journal of Power Sources 196 (2011) 4236−4241.
[22] D. Sebastián, J.C. Calderón, J.A. González-Expósito, E. Pastor, M.V. Martínez-Huerta, I. Suelves, R. Moliner, M.J. Lázaro, International Journal of Hydrogen Energy 35 (2010) 9934−9942.
[23] M. Götz, H. Wendt, Electrochimica Acta 43 (1998) 3637−3644.
[24] N. Fujiwara, K. Yasuda, T. Ioroi, Z. Siroma, Y. Miyazaki, Electrochimica Acta 47 (2002) 4079−4084.
[25] V. Celorrio, L. Calvillo, M.V. Martinez-Huerta, R. Moliner, M.J. Lazaro, Energy & Fuels 24 (2010) 3361−3365.
[26] L. Calvillo, M.J. Lázaro, E. García-Bordejé, R. Moliner, P.L. Cabot, I. Esparbé, E. Pastor, J.J. Quintana, Journal of Power Sources 169 (2007) 59−64.
[27] X. Wang, I.M. Hsing, Electrochimica Acta 47 (2002) 2981−2987.
[28] J.R.C. Salgado, F. Alcaide, G. Álvarez, L. Calvillo, M.J. Lázaro, E. Pastor, Journal of Power Sources 195 (2010) 4022−4029.
[29] S. Pérez-Rodríguez, M. Corengia, G. García, C.F. Zinola, M.J. Lázaro, E. Pastor, International Journal of Hydrogen Energy 37 (2012) 7141−7151.
[30] L. Jiang, G. Sun, X. Zhao, Z. Zhou, S. Yan, S. Tang, G. Wang, B. Zhou, Q. Xin, Electrochimica Acta 50 (2005) 2371−2376.
[31] F. Maillard, M. Eikerling, O.V. Cherstiouk, S. Schreier, E. Savinova, U. Stimming, Faraday Discussions 125 (2004) 357−377.
[32] S. Wang, S.P. Jiang, T.J. White, J. Guo, X. Wang, Journal of Physical Chemistry C 113 (2009) 18935−18945.
[33] O.V. Cherstiouk, P.A. Simonov, E.R. Savinova, Electrochimica Acta 48 (2003) 3851−3860.
[34] B.E. Hayden, D. Pletcher, J.-P. Suchsland, L.J. Williams, Physical Chemistry Chemical Physics 11 (2009) 9141−9148.
[35] F. Maillard, S. Schreier, M. Hanzlik, E.R. Savinova, S. Weinkauf, U. Stimming, Physical Chemistry Chemical Physics 7 (2005) 385−393.
[36] A. Moore, V. Celorrio, M.M. de Oca, D. Plana, W. Hongthani, M.J. Lazaro, D.J. Fermin, Chemical Communications 47 (2011) 7656−7658.
[37] Z. Jusys, J. Kaiser, R.J. Behm, Langmuir 19 (2003) 6759−6769.